UDC 544.65

L.O. Snizhko, N.L. Gurevina, O.O. Kalinichenko, V.O. Holovenko, K.V. Roienko

EVALUATION OF THE THERMOCHEMICAL REACTIONS IN THE MICRO-DISCHARGES DURING PLASMA ELECTROLYTIC OXIDATION OF ALUMINIUM

Ukrainian State University of Chemical Technology, Dnipro, Ukraine

Plasma electrolytic oxidation of lightweight metals performed in water-based solutions is usually accompanied by both the release of a large volume of gases (mainly H_2 and O_2) and heat emission. Today, the existing electrochemical concepts that tend to explain the oxidation mechanisms involved in the metal conversion under the plasma electrolytic oxidation discharge regime do not provide a clear explanation about these phenomena. In this paper, the critical role of the exothermic thermochemical reactions that occur in micro-discharges between the metal particles emitted from the substrate by discharges and the surrounding water vapour ($2Al+6H_2O=2Al(OH)_3+3H_2+Q$) is considered. This reaction is thermodynamically favourable over a wide temperature range from room temperature to temperatures far in excess of the melting point of aluminium (660^0C). This means that the main product of the reaction between dispersed aluminium and water is aluminium hydroxide $Al(OH)_3$. At the same time, conditions realised in spark discharges allowed forming also Al_2O_3, because it is the most stable product at high temperatures. Comparison between the calculated amount of aluminium oxide, performed using the characteristics of individual discharges, and experimental results taken from the literature revealed that the thermochemical reactions is mainly responsible for both the large amount of gas release and heat emission during the plasma electrolytic oxidation of aluminium.

Keywords: plasma electrolytic oxidation; hydrogen release, growth kinetics, micro-discharges; aluminium.

DOI: 10.32434/0321-4095-2019-126-5-135-142

Introduction

Various aspects of the mechanism of plasma electrolytic oxidation (PEO) have been studied, such as correlation between voltage, time of electrolysis and spark quantity at different current densities and regimes, characterisation of light emission during electrolysis and spark parameters, measurements of anodic gas amount evolved during electrolysis, elemental and phase analysis of coatings, measurements of the mass, thickness and porosity of the coatings.

To investigate the true mechanisms involved in the PEO process, the complex of experiments devoted to the investigation of material balance of this process has to be done in the similar experimental conditions. Unfortunately, such complex studies are not known to us. Until now, the nature of non-Faradaic gas evolution, high hydrogen light emission and mechanism of heat generation remains unclear.

In this study, attention is paid to the thermochemical processes that take place in micro-discharges, to which very few articles have been devoted, to the authors' knowledge. The main idea of this paper is to propose a model which could explain the main role of the water conversion of the dispersed metal particles ejected from the substrate into the micro-discharges. We proposed that the low-voltage metal anodising which occurs before sparks ignition is only responsible for the formation of a thin primary dielectric oxide layer which thereafter suffers from the subsequent breakdown events. During sparking in anodic polarization, the thermochemical conversion of the metal substrate provides the main quantity of aluminium hydroxide and results in the main quantity of hydrogen in anodic gases [1]. Therefore, the purely electrochemical mechanism cannot explain either the quantity or the composition of the gas released at the stage of sparking. At the

same time, the ability of activated aluminium and its alloys to reduce water to hydrogen is well-known from numerous research in the hydrogen production technologies [2].

The goal of this paper is to relate the coating growth mechanisms to the discharge characterization.

Experimental data

The corresponding experimental data taken into consideration were obtained from the analysis of literature given below.

The cumulative number of micro-discharges that appear during a PEO treatment was shown to be at least two orders of magnitude lower than the population density of pores on the surface of the final coating. Increased processing time results in coarsening of the coating surface due to the formation of relatively large pores. The diameter of the light-emitting region was estimated between 50 μm (for coating thickness of 5 μm) and 150 μm (for coating thickness of 50 μm). This difference was connected with the formation of multiple discharges and the net of channels to release the gases formed during plasma oxidation [3]. Predicted radius of the gas bubble, r, at the point of peak current in individual discharge lying in the range of 0.01 to 0.07 A·discharge^{-1} was estimated between 2–40 μm [4].

Some different results, namely drop in micro-discharge density from $3.8 \cdot 10^{11}$ discharges·m^{-2} to $1 \cdot 10^{10}$ discharges·m^{-2} during a processing period of 2160 s were observed by Shen et al. [5]. It was established that the population of craters was about $1 \cdot 10^{10}$ craters·m^{-2} at the discharge rate of $1 \cdot 10^{8}$ discharges·m^{-2}·s^{-1}, so in two orders higher. The number of pores was shown to decrease significantly with the increase in the film thickness.

Our calculations were based on a results obtained by authors [3]. In cited work, estimation of discharge parameters has been done by video images recorded by using a Photron SA1.1 camera which allowed studying microdischarges evolution either along the current period or over the processing time. The sampling rate was set at 125000 frames per second (125 kfps) which corresponds to a time resolution of 8 μs. Under these specific recording conditions, the spatial resolution of the camera was set at 0.017 mm^2 which is much lower (by a factor of ~15) than the minimum area of microdischarges. The number density was estimated as a function of the processing time.

It was shown that the substrate consumption rate of 10 nm·s^{-1} corresponds to 10 μm^3·mm^{-2}·ms^{-1}, so one discharge consumes ~10 μm^3 of Al (creating ~15 μm^3 of coating). In terms of energy consumption, this represents ~10^{13} J·m^{-3} of coating (since the energy of a discharge is in the range of ~100–200 μJ). The single spark produces the individual gas bubble with the minimal radius of ~35 μm.

From Fig. 4,b in ref. [6], the discharge density is ~10^{10} for all frequencies at time=0 and decrease to ~$1.6 \cdot 10^{9}$, ~$1.6 \cdot 10^{9}$ and ~$1.6 \cdot 10^{9}$ for f=100 Hz, 500 Hz, and 900 Hz, respectively. At the same time, authors evaluated the average growth rate of the PEO coatings under different current densities and different current pulse frequencies [7]. It was shown that the current density has a more visible influence on the growth rate than the current pulse frequency. The highest coating growth rate (2.1 μm·min^{-1}) was achieved with the combination of the highest current density (75.7 A·dm^{-2}) and the highest current pulse frequency (900 Hz).

It is well-known that PEO occurs in diluted (1–5 g·L^{-1}) alkaline solutions containing KOH, Na_2SiO_3, Na_3PO_4, and $NaAlO_2$. At the same time, the nature of anion has very weak influence on the dielectric properties and chemical composition of anodic film. In the case of PEO of aluminium in a solution of potassium hydroxide and sodium silicate, the spectra also showed the existence of atomic lines of O, Na and K (from the electrolyte) and Al (from the substrate). Optical emission spectroscopy measurements [8] revealed the strong emission of H_α- and H_β-Balmer lines of hydrogen. Spectra also revealed two distinct regions composed of a central core of high temperature (~$16 \cdot 10^3 \pm 3500$ K) with a high electron density (N_e~$5 \cdot 10^{17}$ cm^{-3}) and a peripheral region, probably extending into the surrounding electrolyte (~$3.5 \cdot 10^3$ K) with a less electron density (N_e~10^{15} cm^{-3}). It was also shown in ref. [9] that in the case of negative pulse polarisation the cathodic discharges have the stronger light emission than the anodic ones which can be explained by their greater energy or, according to our point of view, by an increase in the amount of hydrogen in the gas. Besides that, in the case of titanium, the metal working electrode is gradually worn down and precipitated to the bottom of the cell in the form of fine particles [10], so the destruction must have been caused partly by heat damage.

The model of plasma electrolytic oxidation

Principal assumptions

Taking into account the possible ejection of dispersed metal particles from the electrode surface by the plasma process which has been confirmed by morphology and composition of the coating, the following thermochemical reactions can occur between activated metal particles (for example, Al)

and water vapour [11]:

$$2Al + 6H_2O \rightarrow 2Al(OH)_3 + 3H_2 + Q_1; \quad (1)$$

$$2Al + 4H_2O \rightarrow 2AlOOH + 3H_2 + Q_2; \quad (2)$$

$$2Al + 3H_2O \rightarrow Al_2O_3 + 3H_2 + Q_3, \quad (3)$$

where Q_1=16.3 kJ·g^{-1}, Q_2=15.5 kJ·g^{-1} and Q_3=15.1 kJ·g^{-1}, respectively.

From thermodynamic point of view, the reaction (1) is more possible due to highest heat effect. All these reactions start at 300^{0}C.

In comparison, the heat emitted during conventional non-sparking oxidation of aluminium is only 3.1 kJ·g^{-1} [3].

The additional heat can be produced by the thermal transformation of aluminium hydroxide to oxide which starts at 300^{0}C:

$$Al(OH)_3 \rightarrow 0.5Al_2O_3 + 1.5H_2O + Q_5, \quad (4)$$

where Q_5=4.2 kJ·g^{-1}.

As a general rule, direct reactions between Al and H_2O at the room conditions are impossible because of the existence of a thin coherent and well adherent oxide layer which prevents these reactions to occur. Therefore, reactions (1)–(3) can occur after the removal and/or destruction of the outer hydrated surface layer which requires the surface to be activated. This activation occurs in alkaline media which results to formation of soluble aluminates:

$$2Al^* + 6H_2O + 6OH^- \rightarrow$$
$$\rightarrow 2[Al(OH)_6]^{3-} + 3H_2 + Q_6. \quad (5)$$

It has been shown [12] that on the first stage of PEO (simple anodising) the oxide films growth on aluminium by $A1^{3+}$ egress and O^{2-}/OH^- ingress diffusion across the film. As the voltage increases, the efficiency of film formation decreases which can be associated with non-uniform film growth, related to local heating and current concentration at the metal/oxide interface. The formation of «inter-connected channels» within the oxide film reveals places of local current concentration. Local heating causes the generation of metal nanoparticles and vapour. The contact area between electrode and plasma is limited to spots of several square microns cross section. Due to Joule heating and ionic impact, these spots are heated very quickly, causing the material to melt and partly evaporate. Oxide film formed in the electrolyte of pH 11 to the breakdown voltage consists of Al_2O_3 depth of about 70 nm and presumably arising from the development of $Al(OH)_3$.

Continuous evaporation expands from the electrode at the temperature ~1·10^4 K and velocity of ~10^3 m·s^{-1} [13]. As the coating thickness increases, there is a tendency for the light emission to have a larger radius and greater intensity with thicker coatings. The diameter of the light-emitting region appears to vary from ~50 μm for a thin (5 μm) coating to ~150 μm for a thicker (~50 μm) coating. It may be that these dimensions relate primarily to the gas bubble forming above the channel, rather than to its core within the coating.

Tomographic reconstruction of the pore structure around a typical discharge channel (with a diameter of ~50 μm) revealed that it extended almost through the entire coating thickness (~100 μm in this case) to the substrate, where there was an oxide layer a few microns in thickness and bubbles reach radii of 500 μm within periods of 100 μs. It was proposed that bubbles consist of water (electrolyte) vapour. One part of the vapour will deposit on the electrode; other part disappears either by radial expansion of the vapour cloud, energy loss and/or by getting into the electrolyte. The high temperature and velocity of the vapour jet guarantees rapid expansion and hence very high cooling rates and small particles can be seen for spark generation.

To simplify the calculations, we have made following assumptions:

– one discharge creates one particle of dispersed metal which interacts with water vapour according to the stoichiometric equation (1) as a most likely;

– diameter of pore remained after ejection of Al is 10 times less than the radius of gas bubble.

Hydrogen volume released and mass of aluminium ejected in a single discharge

To support our hypothesis about the predominant role of reaction (1) in discharges and to estimate the volume of hydrogen formed by this reaction, we used the experimental data obtained by Martin et al. [6]. Values from Fig. 6,a [6] were rebuilt in coordinates r (radius) versus n (density of discharges) and data from Fig. 4,a [6] were approximated by the logarithmic equations (Table).

Dependences of micro-discharge density versus time of electrolysis at different current densities are presented in Fig. 1.

Substitution of the equations n=f(t) from the right side of Table into the left one (r=f(n)) made it possible to obtain the dependences r=f(t) for different current densities (Fig. 2). One can see that the higher the current density and time of electrolysis, the larger

the radius of discharges.

The relationships between the radius (r) and the density (n) of micro-discharges and the time of electrolysis (t)

r=f(n)	n=f(t)
r_1=–0.051ln(n_1)+0.987	n_1=–9770ln(t)+911511
r_2=–0.0676ln(n_2)+1.197	n_2=–200000ln(t)+1000000
r_3=–78.152ln(n_3)+1277	n_3=–100000ln(t)+832776

Note: indexes 1, 2 and 3 correspond to current densities 12.6, 37.9 and 63.1 A·m^{-2}, respectively.

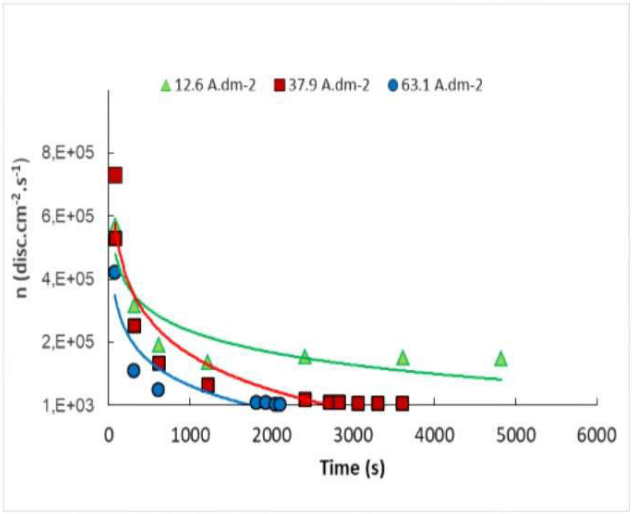

Fig. 1. Density of discharges as function of the processing time of electrolysis at different current densities applied to the electrodes

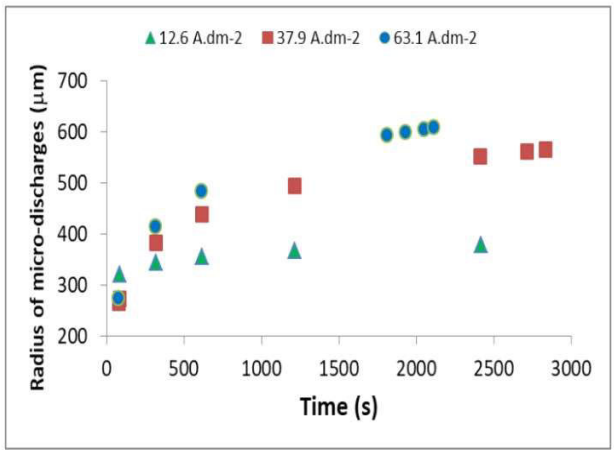

Fig. 2. Estimation of the radius of discharges as function of the processing time at different current densities applied to the electrodes

Taking into account the number of discharges estimated by Martin et al. [6], the rate of gas release u (dm^3·cm^{-2}·s^{-1}) was estimated according to the following equation:

$$u = n \cdot v_g, \quad (7)$$

where

$$v_g = \frac{4}{3}\pi r^3. \quad (8)$$

Results of these calculations are given in Fig. 3.

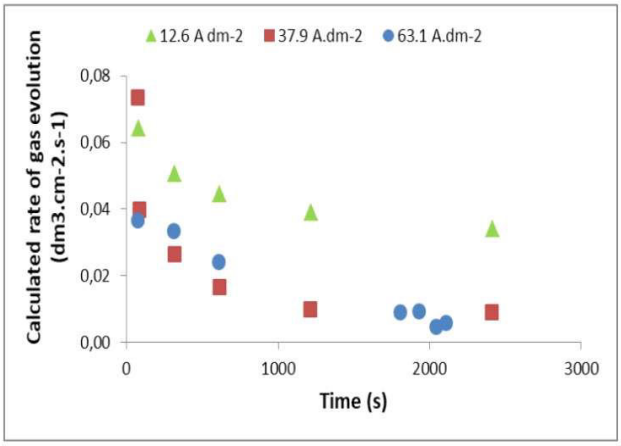

Fig. 3. Calculated rate of gas evolution in sparks as a function of the processing time at different current densities applied to the electrodes

In accordance with our measurements [14], the content of hydrogen in anodic gases achieves 60 vol.% and the rate of anodic gases release is between (0.01–0.04) dm^3·cm^{-2}·s^{-1} in the range of current densities of 5–35 A·dm^{-2}. So, we can see a good coincidence between calculated and experimental results.

It was shown [1] that the ratio «hydrogen/oxygen» in anodic gas is in the range 1.67–1.76 and depends on the current density. The main sources of hydrogen are water thermolysis and reaction (1). To estimate the role of reaction (1) in hydrogen production, the stoichiometric relation was used and the mass of aluminium dispersed in a single sparks m_{Al} (g) was calculated by the equation:

$$m_{Al} = 0.1 \cdot 0.6 \cdot \frac{2}{3}\frac{\upsilon_{H_2}}{V_{mol}} A_{Al}, \quad (9)$$

where A_{Al} is the atomic mass of aluminium (g·mol^{-1}); V_{mol}=22.4 (dm^3·mol^{-1}) is the molar gas volume at the normal conditions (temperature of 273 K and pressure of 101325 Pa); υ_{H_2} is the volume (dm^3) of a gas bubble calculated from the radius of visible

discharges such as 0.1r; and 0.6 is the coefficient which corresponds to the H_2 content in anodic gas.

In these calculations, we used the normal conditions because gas bubbles growth without substantial increase in either pressure or temperature within the local volume, so with the some approximation it was considered that the peak over-pressure within it is relatively low (of the order of 1 atm).

In this regard, the estimated mass of dispersed aluminium produced by a single spark was calculated by formula (9) and presented in Fig. 4.

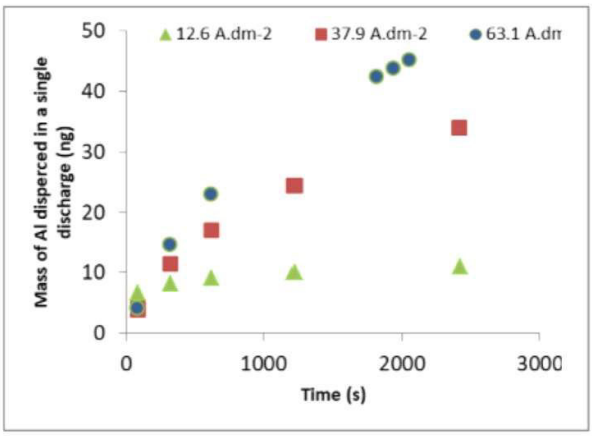

Fig. 4. Estimation of the mass of Al particles dispersed by a single micro-discharge as a function of the processing time at different current densities applied to the electrodes

Nomine et al. [3] supposed that the mass of Al which is converted into oxide and stay at the electrode in the form of oxide is approximately ~0.03 ng per one discharge. This value allowed us to calculate the reaction yield during electrolysis such as 0.1–0.7% at all current densities. The highest yield belongs to the initial period of time and the lowest one corresponds to the end of electrolysis (2600 s). So, one can propose that the rest part of aluminium converted by water produces different forms of aluminium hydroxide.

At the first glance, the data shown in Fig. 3 seem to be contradictory, since the rate of gas evolution decreases with increasing the current density. In addition, the rate of gas evolution sharply decreases with the time of electrolysis. Nevertheless, these data reflect the decrease in the density of micro-discharges and can explain the effectiveness of high current densities towards oxide growth. One can see that the lesser the current density, the higher the rate of the conversion Al to hydroxide (reaction (1)) or soluble forms (reaction (6)).

With the oxide growth, the content of Al significantly reduces and the reaction rate also decreases. The temperature has a significant influence on Al–H_2O reaction. It was shown [15] that the maximal reaction rates ($cm^3 \cdot s^{-1}$) at 60^0C, 70^0C and 80^0C are 0.048 $cm^3 \cdot s^{-1}$, 0.146 $cm^3 \cdot s^{-1}$ and 0.333 $cm^3 \cdot s^{-1}$, respectively. One can see that our data corresponds to the rates obtained at the minimal temperatures.

In accordance with the data obtained, the sequence of events in plasma electrolysis can be described as follows. The electron avalanching leads to the formation of conducting channels with a few nanometres in diameter, which trigger the breakdown. Once such conducting channels form, the subsequent development of the event is determined by thermal effects caused by the current runaway or discharge of the electrostatic energy stored in the specimen through the channels. The electrochemical reactions supported this process are accompanied by the aluminium ionisation and release of gaseous oxygen. In this stage of electrolysis, the discharges of the stored energy through the channels are not sufficiently serious to cause local evaporation of the film material, but instead it leads to the generation of sufficient heat raised to a level at which thermal breakdown is inevitable, i.e. the local temperature rises to such a level that ionic conductivity increases to give current runaway. New conducting channels are most likely to form in the immediate vicinity of the previous channels where the temperature rise is the greatest. Up to this stage, development of the event may not be accompanied by sparking and the short bursts of gas, possibly steam and/or oxygen. More serious discharges accompanied by sparking through the fused channel cause local evaporation of the film material constituting the channels and thereby leaving a hole. The bottom of the hole thus produced may be healed at very high current density and temperature. In addition, the impact of sparking may cause radial propagation of cracks from the centre of the destruction. The discharges through these channels may eventually cause a massive evaporation of the film material producing a pit a few microns in size, attended by a visible and intense sparking. Impact of such sparking may cause more extensive cracks to propagate radially outwards. Both the bottom of the pit and cracks caused by the sparking are healed again at very high current density and temperature, resulting in thicker film formation.

Comparison between heat released by power supply and reaction (1) during sparking

In accordance with our calculations, the energy released by individual discharge q_{el} ($J \cdot discharge^{-1}$)

can be calculated as

$$q_{el} = \frac{i \cdot U \cdot t}{n}, \qquad (10)$$

where i, U, t and n are the current density ($A \cdot m^{-2}$), voltage (V), time (s) and the number of discharges in the current moment of electrolysis, respectively.

The values of q_{el} were estimated in the range of $(1.2-3.7) \cdot 10^{-4}$ at 12.6, $(2.2-120.0) \cdot 10^{-4}$ at 37.9 and $(8.2-580) \cdot 10^{-4}$ at 63.1 $A \cdot dm^{-2}$, respectively. These results coincide with the known data [3] where q_{el} was found in the range of ~ $(1.0-2.0) \cdot 10^{-4}$ $J \cdot discharge^{-1}$ that corresponds to the total energy consumption closed to ~10^{13} $J \cdot m^{-3}$. So, our results are in satisfactory agreement with data obtained at low current densities.

Using the value Q_1 which is the heat released by the reaction (1), the energy q_{tr} of aluminium conversion can be calculated according to the following equation using data taking for m_{Al} from Fig. 4:

$$q_{tr} = m_{Al} \cdot Q_1. \qquad (11)$$

The calculated results are shown in Fig. 5.

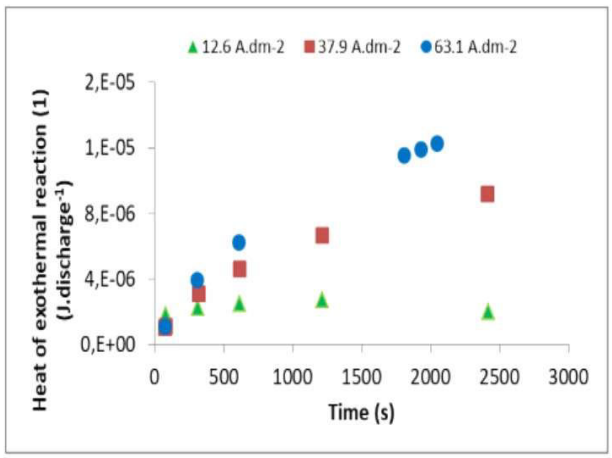

Fig. 5. The energy of exothermal reaction (1) as a function of processing time at different current densities applied to the electrodes

The fraction of the energy (η, %) released in reaction (1) in the total energy consumed from the power supply was calculated as follows:

$$\eta = \frac{q_{tr}}{q_{el}} 100. \qquad (12)$$

The obtained results are shown in Fig. 6.

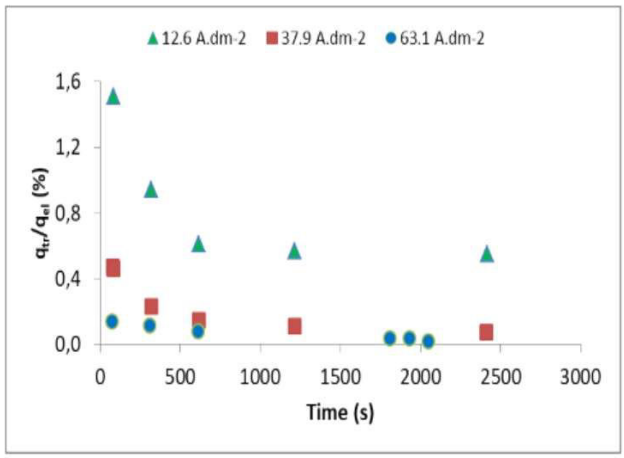

Fig. 6. The fraction of the energy released in micro-discharges by reaction (1) in the total energy consumed from the power supply at different current densities applied to the electrode

Surprisingly, the higher the current density, the lesser the fraction of energy released by reaction (1) in the total energy consumed from the power supply.

It is clear that the PEO process is accompanied by spark discharges with the temperature of several thousand centigrade, so it is impossible to compare the real heating provided by discharges with the heat effect of chemical reaction (1).

Conclusions

It was proposed that the main role in plasma electrolytic oxidation in the stage of sparking belongs to the thermochemical conversion of metal by water vapour that provides the main quantity of gases with the primary concentration of hydrogen in them. The amount of anodic gases was calculated from optical measurements of number and sizes of discharges (literature data). The volume of possible gas bubble, which, in its turn, was calculated from the radius of light spots, was used for the estimation of hydrogen evolution rate. Good correlation between calculated and experimental results was found. Taking into account the content of hydrogen (60–70 vol.%) in anodic gases, the possible amount of aluminium dispersed in individual sparks was calculated according to the reaction $2Al + 6H_2O = 2Al(OH)_3 + 3H_2 + Q_1$. It was shown that the reaction yield for Al conversion during thermochemical stage of electrolysis is approximately 0.1–0.7% at all current densities.

It was also found that the heat released in sparks by exothermic thermochemical reaction is near to 1% of the total energy input.

Acknowledgments

The authors thank to Prof. G. Henrion and Dr. J. Martin (Institut Jean Lamour, CNRS-

Universitй de Lorraine, France) for helpful discussions.

Funding: the work was funded by the grant for young scientists of the Ministry of Science and Education of Ukraine No. 17/170190 «Functionalization of oxide-ceramic coatings on light alloys for objects of various purposes».

REFERENCES

1. *Investigation* of gaseous by-products of interaction of in-liquid plasmas with al during plasma electrolytic oxidation / Yerokhin A., Gao Y., Gonzalvo Y.A., Snizhko L. // Proceedings of the - International Conference on Metallurgical Coatings & Thin Films (ICMCTF'15). – US, Sun Diego, 2015.

2. *A review* on hydrogen production using aluminum and aluminum alloys / Wang H.Z., Leung D.Y.C., Leung M.K.H., Ni M. // Renew. Sustainable Energy Rev. – 2009. – Vol.13. – P.845-853.

3. *High* speed video evidence for localised discharge cascades during plasma electrolytic oxidation / Nomine A., Troughton S.C., Nomine A.V., Henrion G., Clyne T.W. // Surf. Coat. Technol. – 2015. – Vol.269. – P.125-130.

4. *Dunleavy C.S., Curran J.A., Clyne T.W.* Self-similar scaling of discharge events through PEO coatings on aluminium // Surf. Coat. Technol. – 2011. – Vol.206. – P.1051-1061.

5. *Microstructure*, temperature estimation and thermal shock resistance of PEO ceramic coatings on aluminum / Shen D.-J., Wang Y-.L., Nash P., Xing G.-Z. // J. Mater. Process. Technol. – 2008. – Vol.205. – P.477-481.

6. *Effects* of electrical parameters on plasma electrolytic oxidation of aluminium / Martin J., Melhem A., Shchedrina I., Duchanoy T., Nomine A., Henrion G., Czerwiec T., Belmonte T. // Surf. Coat. Technol. – 2013. – Vol.221. – P.70-76.

7. *Effect* of cathodic micro-discharges on oxide growth during plasma electrolytic oxidation (PEO) / Nomine A., Martin J., Henrion G., Belmonte T. // Surf. Coat. Technol. – 2015. – Vol.269. – P.131-137.

8. *Characterisation* of discharge events during plasma electrolytic oxidation / Dunleavy C.S., Golosnoy I.O., Curran J.A., Clyne T.W. // Surf. Coat. Technol. – 2009. – Vol.203. – P.3410-3419.

9. *Effect* of individual discharge cascades on the microstructure of plasma electrolytic oxidation coatings / Troughton S.C., Nomine A., Dean J., Clyne T.W. // Appl. Surf. Sci. – 2016. – Vol.389. – P.260-269.

10. *Destruction* of coating material during spark anodizing of titanium / Matykina E., Doucet G., Monfort F., Berkani A., Skeldon P., Thompson G.E. // Electrochim. Acta. – 2006. – Vol.51. – P.4709-4715.

11. *Production* of hydrogen in the reaction between aluminum and water in the presence of NaOH and KOH / Porciuncula C.B., Marcilio N.R., Tessaro I.C., Gerchmann M. // Braz. J. Chem. Eng. – 2012. – Vol.29. – P.337-348.

12. *Formation* of amorphous anodic oxide films of controlled composition on aluminium alloys / Habazaki H., Shimizu K., Skeldon P., Thompson G.E., Wood G.C. // Thin Solid Films. – 1997. – Vol.300. – P.131-137.

13. *Cundall C.M., Craggs J.D.* Excitation temperatures in spark discharges // Spectrochim. Acta. – 1957. – Vol.9. – P.68-88.

14. *Analysis* of gaseous products of plasma electrolytic oxidation of aluminum / Golovenko V.A., Kalinichenko O.A., Roenko E.V., Gurevina N.L., Snezhko L.A. // Surf. Eng. Appl. Electrochem. – 2019. – Vol.55. – P.191-196.

15. *Sarkar J., Bhattacharyya S.* Operating characteristics of transcritical CO_2 heat pump for simultaneous water cooling and heating // Arch. Thermodyn. – 2012. – Vol.33. – P.23-40.

Received 4.04.2019

АНАЛІЗ ТЕРМОХІМІЧНИХ РЕАКЦІЙ В МІКРОРОЗРЯДАХ ПРИ ПЛАЗМОВОМУ ЕЛЕКТРОЛІТИЧНОМУ ОКСИДУВАННІ АЛЮМІНІЮ

Л.О. Сніжко, Н.Л. Гуревіна, О.О. Калініченко, В.О. Головенко, К.В. Роєнко

Плазмове електролітичне оксидування легких металів, яке здійснюється в водних електролітах, зазвичай супроводжується інтенсивним газовиділенням (головним чином, H_2 і O_2) і високим тепловим ефектом. Існуючі сьогодні електрохімічні концепції, що пояснюють механізм окислення металів, не дають чіткого пояснення явищ, що відбуваються при плазмовому електролітичному оксидуванні. В даній статті розглядається провідна роль екзотермічних термохімічних реакцій, які можливі при мікророзрядах між частинками металу, який ежектується з металу, і водяною парою, яка оточує зону розряду ($2Al+6H_2O=2Al(OH)_3+3H_2+Q$). З точки зору термодинаміки наведена реакція ймовірна в широкому діапазоні температур – від кімнатної до температури, яка значно перевищує температуру плавлення алюмінію (660°C). Це означає, що основним продуктом реакції між дисперсним алюмінієм і водою може бути гідроксид алюмінію $Al(OH)_3$. У той же час, умови, які виникають в іскрових розрядах, сприяють також формуванню Al_2O_3, оскільки алюміній оксид є найбільш стабільним продуктом при високих температурах. Порівняння кількості алюміній оксиду, розрахованого з використанням характеристик окремих розрядів, і експериментальних результатів виявило, що термохімічна конверсія алюмінію водяною парою відповідальна як за аномальну кількість, так і за вміст водню в анодному газі під час плазмового електролітичного оксидування алюмінію.

Ключові слова: плазмове електролітичне оксидування, кінетика, виділення водню, мікророзряди, алюміній.

EVALUATION OF THE THERMOCHEMICAL REACTIONS IN THE MICRO-DISCHARGES DURING PLASMA ELECTROLYTIC OXIDATION OF ALUMINIUM

L.O. Snizhko* *, N.L. Gurevina, O.O. Kalinichenko, V.O. Holovenko, K.V. Roienko

Ukrainian State University of Chemical Technology, Dnipro, Ukraine

* **e-mail: lsnizhko@gmail.com**

Plasma electrolytic oxidation of lightweight metals performed in water-based solutions is usually accompanied by both the release of a large volume of gases (mainly H_2 and O_2) and heat emission. Today, the existing electrochemical concepts that tend to explain the oxidation mechanisms involved in the metal conversion under the plasma electrolytic oxidation discharge regime do not provide a clear explanation about these phenomena. In this paper, the critical role of the exothermic thermochemical reactions that occur in micro-discharges between the metal particles emitted from the substrate by discharges and the surrounding water vapour ($2Al+6H_2O=2Al(OH)_3+ +3H_2+Q$) is considered. This reaction is thermodynamically favourable over a wide temperature range from room temperature to temperatures far in excess of the melting point of aluminium (660^0C). This means that the main product of the reaction between dispersed aluminium and water is aluminium hydroxide $Al(OH)_3$. At the same time, conditions realised in spark discharges allowed forming also Al_2O_3, because it is the most stable product at high temperatures. Comparison between the calculated amount of aluminium oxide, performed using the characteristics of individual discharges, and experimental results taken from the literature revealed that the thermochemical reactions is mainly responsible for both the large amount of gas release and heat emission during the plasma electrolytic oxidation of aluminium.

Keywords: plasma electrolytic oxidation; hydrogen release, growth kinetics, micro-discharges; aluminium.

REFERENCES

1. Yerokhin A., Gao Y., Gonzalvo Y.A., Snizhko L., Investigation of gaseous by-products of interaction of in-liquid plasmas with al during plasma electrolytic oxidation. *Proceedings of the - International Conference on Metallurgical Coatings & Thin Films (ICMCTF'15)*. US, Sun Diego, 2015.

2. Wang H.Z., Leung D.Y.C., Leung M.K.H., Ni M. A review on hydrogen production using aluminum and aluminum alloys. *Renewable and Sustainable Energy Reviews*, 2009, vol. 13, pp. 845-853.

3. Nomine A., Troughton S.C., Nomine A.V., Henrion G., Clyne T.W. High speed video evidence for localised discharge cascades during plasma electrolytic oxidation. *Surface and Coatings Technology*, 2015, vol. 269, pp. 125-130.

4. Dunleavy C.S., Curran J.A., Clyne T.W. Self-similar scaling of discharge events through PEO coatings on aluminium. *Surface and Coatings Technology*, 2011, vol. 206, pp. 1051-1061.

5. Shen D.-J., Wang Y-.L., Nash P., Xing G.-Z. Microstructure, temperature estimation and thermal shock resistance of PEO ceramic coatings on aluminum. *Journal of Materials Processing Technology*, 2008, vol. 205, pp. 477-481.

6. Martin J., Melhem A., Shchedrina I., Duchanoy T., Nomine A., Henrion G., Czerwiec T., Belmonte T. Effects of electrical parameters on plasma electrolytic oxidation of aluminium. *Surface and Coatings Technology*, 2013, vol. 221, pp. 70-76.

7. Nomine A., Martin J., Henrion G., Belmonte T. Effect of cathodic micro-discharges on oxide growth during plasma electrolytic oxidation (PEO). *Surface and Coatings Technology*, 2015, vol. 269, pp. 131-137.

8. Dunleavy C.S., Golosnoy I.O., Curran J.A., Clyne T.W. Characterisation of discharge events during plasma electrolytic oxidation. *Surface and Coatings Technology*, 2009, vol. 203, pp. 3410-3419.

9. Troughton S.C., Nomine A., Dean J., Clyne T.W. Effect of individual discharge cascades on the microstructure of plasma electrolytic oxidation coatings. *Applied Surface Science*, 2016, vol. 389, pp. 260-269.

10. Matykina E., Doucet G., Monfort F., Berkani A., Skeldon P., Thompson G.E. Destruction of coating material during spark anodizing of titanium. *Electrochimica Acta*, 2006, vol. 51, pp. 4709-4715.

11. Porciuncula C.B., Marcilio N.R., Tessaro I.C., Gerchmann M. Production of hydrogen in the reaction between aluminum and water in the presence of NaOH and KOH. *Brazilian Journal of Chemical Engineering*, 2012, vol. 29, pp. 337-348.

12. Habazaki H., Shimizu K., Skeldon P., Thompson G.E., Wood G.C. Formation of amorphous anodic oxide films of controlled composition on aluminium alloys. *Thin Solid Films*, 1997, vol. 300, pp. 131-137.

13. Cundall C.M., Craggs J.D. Excitation temperatures in spark discharges. *Spectrochimica Acta*, 1957, vol. 9, pp. 68-88.

14. Golovenko V.A., Kalinichenko O.A., Roenko E.V., Gurevina N.L., Snezhko L.A. Analysis of gaseous products of plasma electrolytic oxidation of aluminum. *Surface Engineering and Applied Electrochemistry*, 2019, vol. 55, pp. 191-196.

15. Sarkar J., Bhattacharyya S. Operating characteristics of transcritical CO_2 heat pump for simultaneous water cooling and heating. *Archives of Thermodynamics*, 2012, vol. 33, pp. 23-40.